Journal of the Optical Society of Korea, Vol. 4, No. 2, September 2000, pp. 79-85

Design and Fabrication of a Holographic Solar Concentrator

Tae Youn Hur, Hee Dong Kim, and Man Ho Jeong

Department of Optical Engineering, Chongju University, Chongju 360-764, KOREA

(Received December 17, 1999)

The main purpose of this paper is to present the potential of photovoltaic systems using holographic solar concentrators. A hologram used here focuses light, spectrally splits it and diverts unwanted infrared heat away from the solar cell. The output of the hologram appears as a perpendicular thin spectral line and is displaced to solar cells on both sides. To obtain optimum design conditions we used the coupled wave theory and the vector ray tracing method. The measured data showed that the diffraction efficiency was 75 % and the spectral bandwidth was 350 nm.

I. INTRODUCTION

The simplest type of photovoltaic system, a power generation system from solar radiation, consists of flat silicon panels. The efficiency of such systems is low and amounts to 10% in all [1]. This low efficiency can be increased by tracking the sun and concentrating the incoming radiation by using lenses. Concentrating the incoming radiation increases the efficiency by 10 %, for an overall efficiency of 20–25 %. The main loss of the photovoltaic system efficiency is caused by the difference between the wavelength of the incoming solar radiation and the bandgap wavelength of the solar cell. In other words, photons having wavelength longer than the bandgap can not consume thermal energy and be absorbed, but shorter wavelength photons expend the energy over the bandgap on thermal energy inflicting a loss on the system. Thus by splitting and concentrating the spectrum and using solar cells matched to the splitted wavelengths, the system efficiency can be improved to 30–40 %.

Various conventional optical elements have been used in solar concentrators in photovoltaic systems but there is a very poor potential for practical use. On the other hand, holographic elements are lightweight, durable, flat, economical, multifunctional, and highly suitable for use in a space environment. Thus holography offers an ideal solution to the problems of solar concentration and spectrum splitting for photovoltaic conversion [2].

Fig. 1 shows a schematic diagram of the operation of the holographic solar concentrator (HSC) we constructed. The hologram perpendicular to the incident solar radiation concentrates and spectrally separates the incident light, resulting in a focused, spectrally-dispersed line. The solar cell is vertically located on the focal plane of the hologram. This kind of side focus method, which divers unwanted far-IR and ellimminates shadow and cross coupling effects, can reduce cooling requirements. Thus a highly improved photovoltaic system efficiency, the major advantage of this structure, is achieved [3-6].

In this research, to design and fabricate the HSC as shown in Fig. 1, we analyzed the essential parameters

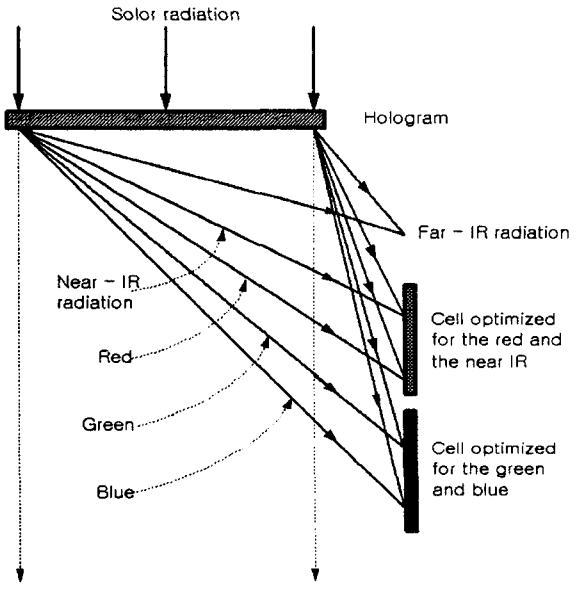

FIG. 1. The configuration of the HSC.

such as recording angle, spectral bandwidth, recording material, and diffraction efficiency by Kogelnik's coupled wave theory. In addition to this theory, vector ray tracing was applied to consider image variation problems resulting from changing the hologram size. Moreover we fabricated an HSC measured the spectral bandwidth and the efficiency, and presented the potential for use as a solar concentrator.

II. THEORY

1. Coupled wave theory

The diffraction efficiency of holographic optical elements (HOE) depends on the wavelength of the incident radiation, as well as on the spectral sensitivity of the photovoltaic cell which converts the light energy into electrical energy. Thus the efficiency of the whole system may be evaluated as the product of the solar spectrum, the HOE diffraction efficiency as a function of wavelength, and the solar cell efficiency as a function of wavelength, i.e.

$$\text{System } \eta = \frac{\int S(\lambda) H_\eta(\lambda) C_\eta(\lambda) d\lambda}{\int S(\lambda) d\lambda}, \tag{1}$$

where S is the solar spectrum, H_η is the hologram diffraction efficiency, and C_η is the solar cell's efficiency. In Eq. (1) we can find that if the solar spectrum and the solar cell efficiency are fixed values, then the photovoltaic system efficiency is proportional to the hologram efficiency. Thus by analyzing the spectral bandwidth and the diffraction efficiency as a function of the hologram recording angle and wavelength we can determine a recording condition with wide spectral bandwidth and high diffraction efficiency. In order to solve those problems we used the two-wave first-order coupled wave theory of Kogelnik.

The efficiency of the lossless transmission hologram by Kogelnik's coupled wave theory is written in the form [7]

$$\eta = \left| -i \frac{\exp(-\Delta\lambda\beta) \sin(\Delta\lambda^2\beta^2 + \nu^2)^{1/2}}{(1 + \Delta\lambda^2\beta^2/\nu^2)^{1/2}} \right|^2, \tag{2}$$

where

$$\nu = \frac{\pi n_1 T}{\lambda_r \cos\theta_B}, \tag{3}$$

$$\beta = \frac{\xi}{\Delta\lambda} = -\frac{1}{\lambda_r} \tan\theta_B \left(\frac{2\pi n_0}{\lambda_r} \right) T \sin\theta_B. \tag{4}$$

In Eq. (4) $2\theta_B$ is an angle between two interfering beams in the recording medium, and T is the emulsion layer thickness. n_0 is the refraction coefficient average value, and n_1 is the modulation amplitude of the refraction coefficient. λ_r is the recording wavelength, and $\Delta\lambda$ is the difference between the recording wavelength and the reconstruction wavelength.

If we define the parameter $Q = 2\pi\lambda d/n\Lambda^2$ as an appropriate measure of grating thickness, because the coupled wave theory gives good results for thick holograms, when $Q \geq 0$, we assume that the value of Q is 10. If we assume the Bragg condition and apply Bragg's law, we can rewrite the new function of $T(\theta_B)$, i.e.

$$T(\theta_B) = \frac{Q\lambda_r}{8\pi n_0 \sin^2\theta_B}. \tag{5}$$

And the spectral bandwidth of the transmission volume hologram is obtained by Eq. (6)

$$\Delta\lambda \approx 2\frac{d\lambda_r \cot\theta_B}{T} = 0.8\pi\lambda_r \cos\theta_B. \tag{6}$$

2. Vector ray tracing equation

To acquire the desired structure of the solar concentrator and the hologram size, we used a vector ray tracing equation, i.e. [8]

$$\hat{n} \times (\hat{r}_i - \hat{r}_c) = m\frac{\lambda_c}{\lambda_r}\hat{n} \times (\hat{r}_o - \hat{r}_r), \tag{7}$$

where $\hat{n}$ is a unit vector normal to the hologram, λ_r is the recording wavelength, λ_c is the reconstruction wavelength, m is the order of diffraction. $\hat{r}_o(L_o, M_o, N_o)$, $\hat{r}_r(L_r, M_r, N_r)$, $\hat{r}_c(L_c, M_c, N_c)$, and $\hat{r}_i(L_i, M_i, N_i)$ whose components are the direction cosines which represent unit vectors of the object beam, the reference beam, the reconstruction beam, and the diffracted beam, respectively.

Fig. 2 shows a coordinates for the vector ray tracing of an HSC. The hologram is located in the $x_h y_h$ plane and its center is at the origin of this plane. The image plane perpendicular to the hologram is parallel to the $x_i z_i$ plane. $O(x_o, y_o, z_o)$, $R(x_r, y_r, z_r)$, $C(x_c, y_c, z_c)$, and $I(x_i, y_i, z_i)$ are the coordinates of the object beam, the reference beam, the reconstruction beam, and the diffracted beam, respectively. $H(x_h, y_h, 0)$ represents the coordinates of a point on the hologram. R_r, R_o, and R_c are the distances from $H(x_h, y_h, z_h)$ to the object beam, the reference beam, and the reconstruction beam, respectively, and R_i is the distance to a diffracted image point.

If we define $I(x_i, y_i, z_i)$ as coordinates of the image point, y_i is a constant representing the location of the image plane, each component of the image point coordinates is obtained by using the following equations:

$$D = \frac{y_i - y_h}{M_i}, \tag{8}$$

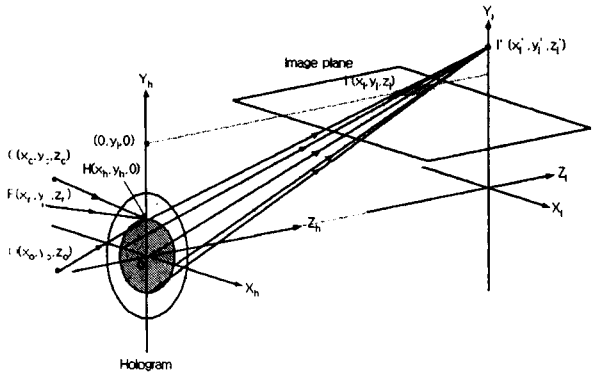

FIG. 2. The coordinates for ray-tracing the HSC.

$$x_i = DL_i + x_h, \tag{9}$$

$$z_i = DN_i + z_h. \tag{10}$$

III. DESIGN OF AN HOE FOR SOLAR CONCENTRATOR

In the design of the HSC we must consider some conditions of the recording angle, the recording wavelength, and the emulsion thickness which are essential to the desired spectral bandwidth and diffraction efficiency.

Fig. 3-(a) shows the spectral bandwidth changes of the hologram with the variation of the angle between two recording beams when $Q = 10$, $\lambda_r = 442, 488, 514$, and 633 nm, and $n_0 = 1.64$. As the recording angle increases, the spectral bandwidth decreases in the form of a cosine function, but at the same recording angle the spectral bandwidth increases with increasing the recording wavelength. If Q is larger than 10, the spectral bandwidth rapidly decreases.

Fig. 3-(b) shows the emulsion thickness variation according to the recording wavelength and the recording angle. As the recording angle increases, the thickness decreases sharply. In contrast the variation of the thickness with changes in recording wavelength is very small. If Q is larger than 10, the thickness becomes very large.

Fig 3-(c) shows the diffraction efficiency of the lossless transmission volume hologram versus the recording wavelength when $T = 4\ \mu$m, $2\theta_B = 21°$, $\nu = \pi/2$. As the recording wavelength becomes larger, the hologram has the higher efficiency in a broader spectral range

Therefore, in the fabrication of the HSC to get wider spectral bandwidth (over 95 % of the maximum spectral bandwidth) and higher diffraction efficiency we must satisfy the conditions, $Q = 10$, $\lambda_r = 633$nm,

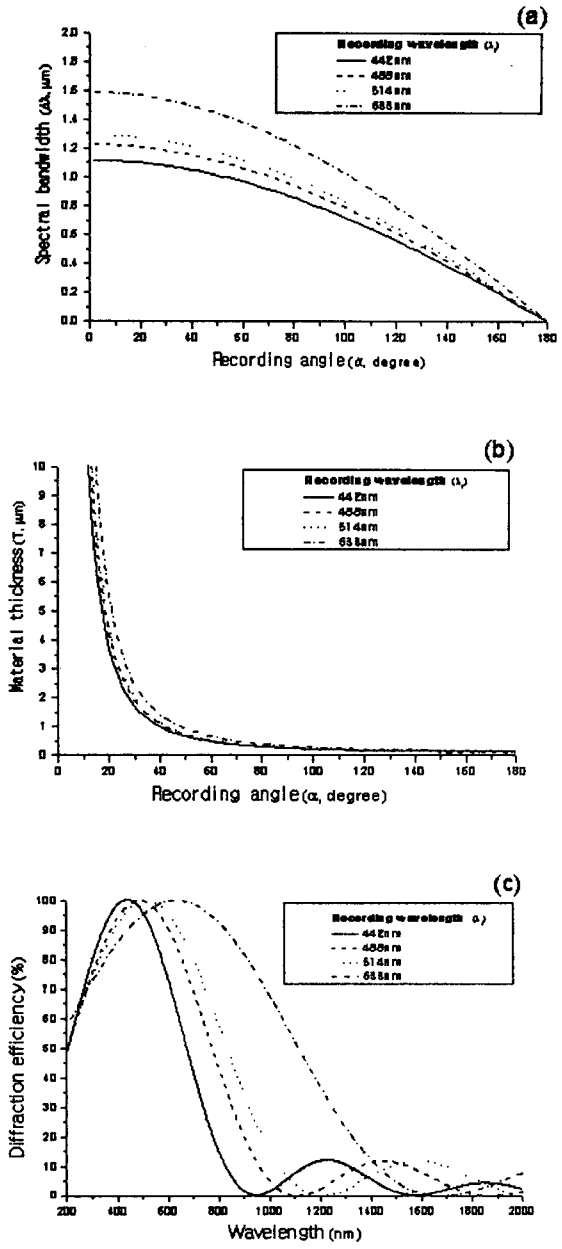

FIG. 3. The variation of (a) the spectral bandwidth, (b) emulsion thickness with the recording angle and the recording wavelength, and (c) the diffraction efficiency changes with the recording and the reconstruction wavelength.

$2\theta_B = 20° - 35°$, and $T = 1.5\mu$m $- 5\mu$m. Applying the recording conditions previously acquired to the ray tracing method, we need to analyze some design parameters for the fabrication of the HSC. The incident light is concentrated and spectrally separated by the concentrator, and then is linearly focused on the image plane (that is, solar cell). The linearly focused spectrum affects the size of the solar cell and of the

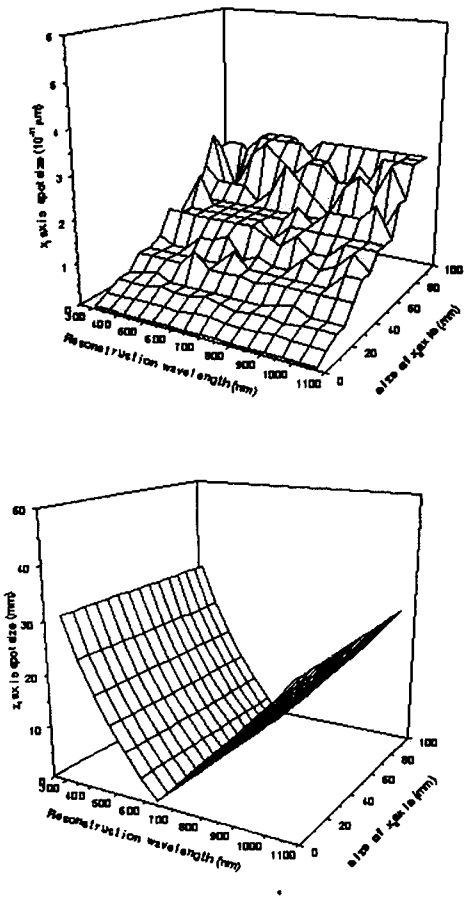

FIG. 4. The spot size variation of the x_i and the z_i axis on the image plane with the hologram size of x_h axis.

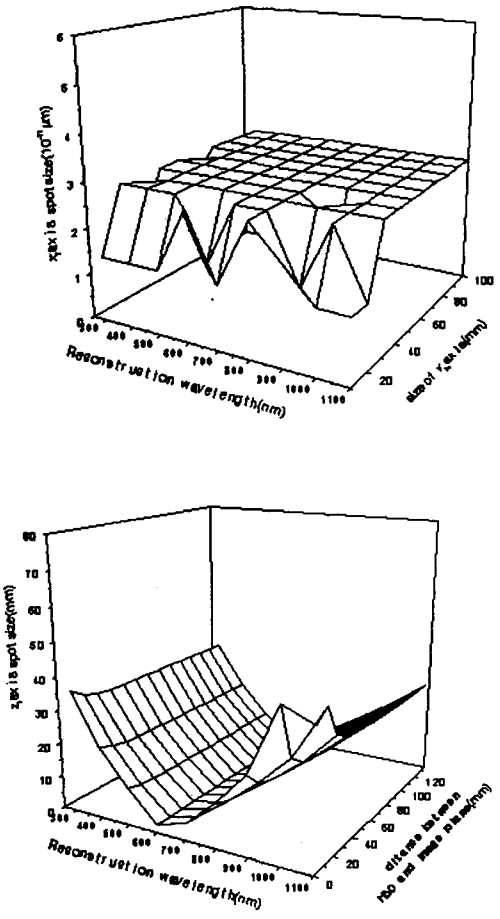

FIG. 5. The spot size variation of the x_i and the z_i axis with the hologram size of y_h axis.

whole system. Thus analysis of the design parameters, for example the concentrator size and the location of the image plane (the location of the solar cell), is necessary.

Figs. 4, 5, and 6 represent the results of analyzed design parameters when the reconstruction wavelength, hologram size on the x_h axis and y_h axis, and y-axis distance between the hologram and the image plane are 300 nm – 1100 nm, 0 – 100 mm, and 0 – 120 mm, respectively. In this case the recording wavelength, reference beam angle, and object beam angles are 633 nm, 0°, and 21°, respectively. Figs. 4 and 5 show the reconstructed spot size of the image on the $x_i z_i$ plane versus the reconstruction wavelength when holograms have various sizes on the $x_h y_h$ plane. Here the spot size is the geometrical size for which the diffraction limit is not considered. In these two figures we know that while the spot size variation on the x_i axis with the change of the reconstruction wavelength is very small, the variation on the z_i axis is several tens of mm and relatively larger than on the x_i axis. When we compare the variation of the spot size on the z_i axis according to the hologram size on the x_h and the y_h axis, we, thus, know that the spot size on the z_i axis is more affected not by the size on the x_h axis but by the size on the y_h axis. This means that the hologram size variation on the y_h axis influence the spot size. Thus we can conclude that the y_h axis has strong relation to the size of the solar cell.

Fig. 6 represents the spot size variation with the y-axis distance between the concentrator and the image plane, when the image plane is perpendicular to the location of the concentrator. The variation assumes the form of a V and if the image plane is close to the concentrator, the spot size in the longer wavelength range has a tendency to increase due to diffraction.

Through the above analyzed results we designed a HSC having the structure as shown in Fig. 7. For the recording wavelength of 633 nm and the recording angle of 21°, the size of HSC and solar cell are 10mm × 410 mm, and 100 mm × 55 mm, respectively. The y-axis distance between the HSC and solar cell is 55 mm. Fig. 8 represents the simulated spot image on the image plane obtained from the designed structure.

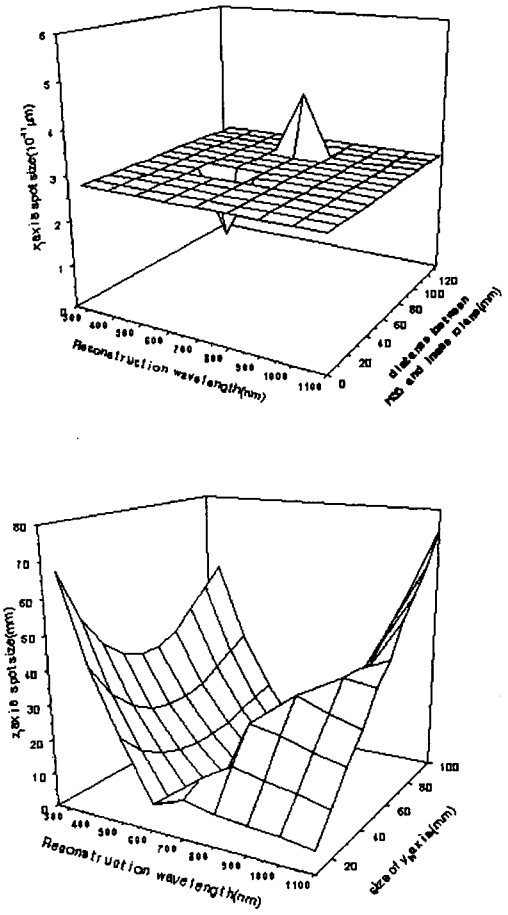

FIG. 6. The spot size variation of the x_i and the z_i axis on the image plane with the distance between the hologram and the image plane along the y axis.

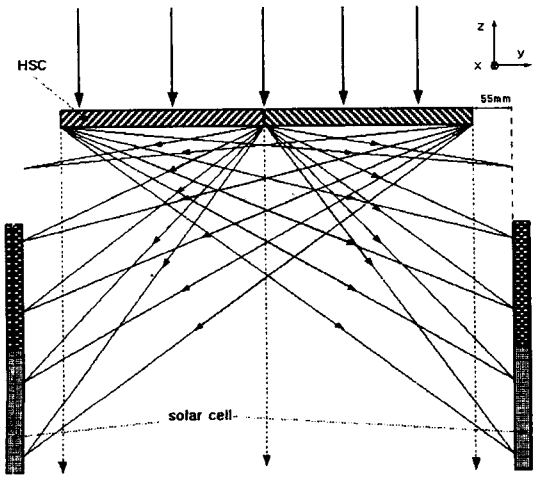

FIG. 7. The designed configuration of the HSC.

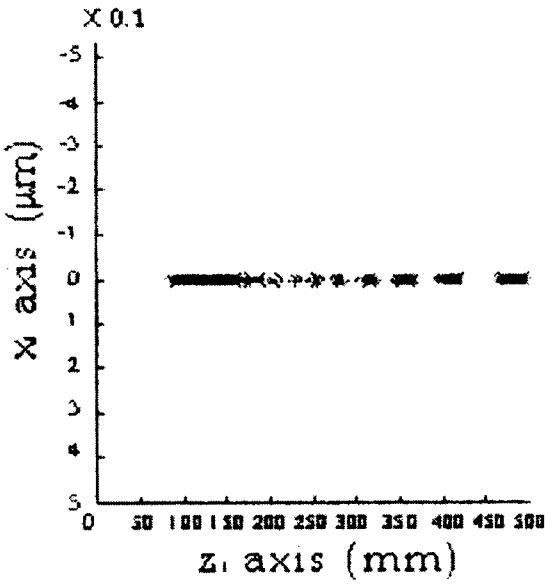

FIG. 8. The trace of reconstruction wavelengths on the image plane.

IV. FABRICATION AND EXPERIMENTAL RESULTS

Experimental setup for the HSC with both functions of focusing and spectral separation designed by the coupled wave theory and the vector ray tracing equation is sketched in Fig. 9.

The light source was a He-Ne laser of 633 nm. $\lambda/2$ plates and polarizing beam splitter (PBS) were used for making two beams of the same intensity and polarization direction. The off-axis holographic lens was formed by the interference between the collimated reference beam incident perpendicular to the recording material and the spherical object beam of α with that material. The reference beam traveled through spatial filter 1 (SF1) and a lens. The object beam traveled through SF2. By locating a diffuser on the backside of the recording plate, the backside reflection was minimized.

We used a silver-halide plate (Agfa 8E75HD) for a refractive index modulation type of hologram. The plate was placed at the position of the recording material in Fig. 9 and after exposure by about 100 μW/cm^2 it was chemically processed by the fixation free rehalogenating bleaching method [9]. According to this method holograms are bleached directly after development without fixing, leaving the unexposed silver-halide crystals in the emulsion, so those phenomena of the shrinkage of the emulsion caused by removing the silver-halide and noise occurred in the interference fringe can be reduced. In addition the diffraction efficiency was improved by including the alcohol dry in the chemical process.

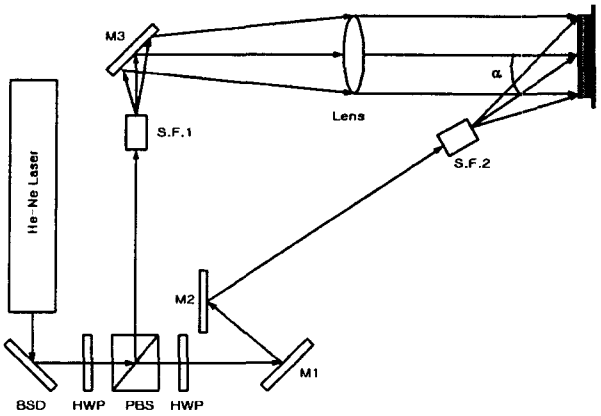

FIG. 9. The experimental setup for fabricating a HSC.

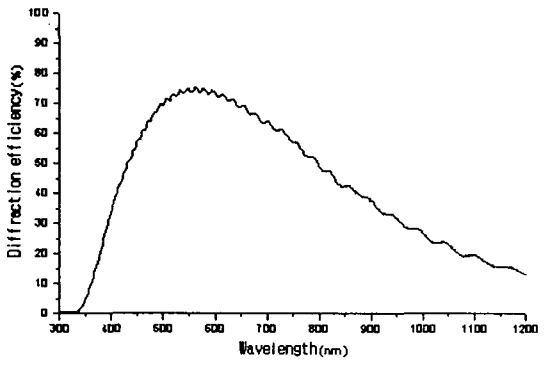

FIG. 10. The diffraction efficiency of the fabricated hologram.

Fig. 10 represents the measured diffraction efficiency of the fabricated hologram. The maximum efficiency was about 75 % at 560 nm, and the reconstructed wavelength shifted from $633nm$ of the recording wavelength to $560nm$ by the change of the emulsion thickness occurred in the processing. The spectral bandwidth was about 350 nm.

The image shown in Fig. 11 was reconstructed when the light from a Halogen lamp was vertically incident to the fabricated HSC. That is a linear type agreed well with the spot image shown in Fig. 8. Since the image quality was a less important factor, the spot image for each wavelength was not measured.

V. CONCLUSIONS

For increasing the efficiency of a photovoltaic system, an HSC performing both functions of focusing and splitting was fabricated. The optimization design conditions of the recording wavelength, the recording angle, and the emulsion thickness for the spectral bandwidth and the diffraction efficiency of the solar concentrator were presented by coupled wave theory. When the angle between two recording beams $\alpha = 20^o - 35^o$, the emulsion thickness $T = 1.5\ \mu\text{m} - 5\ \mu\text{m}$, and the recording wavelength $\lambda_r = 633$ nm, high diffraction efficiency was achieved in the wide spectral bandwidth. Through the vector ray tracing method considering those conditions, we analyzed the shape and configuration of the solar concentrator and then designed the concentration system. The sizes of HSC and solar cell were 100 mm × 55 mm, 10 mm × 410 mm, respectively, and the y-axis distance between them was 55 mm.

We fabricated an HSC by the design specifications and then measured the diffraction and the spot image. The HSC fabricated on a silver-halide plate represented diffraction of 75 % and spectral bandwidth of 350 nm by the fixation free rehalogenating bleaching and the alcohol dry method. And the same spot image coincident with our design was observed.

In our research the length of the solar cell was somewhat large because the recording angle was small. To reduce the length the recording angle must be larger. And the diffraction efficiency over 90 % can be achieved if we use the material with high modulation property of the refractive index instead of the silver-halide plate.

It is expected that the power generation cost of a photovoltaic system containing the HSC reaches the level of a commercial system by the advantages of highly focusing the solar rays, decreasing the reflection loss, eliminating the shadow effect and the cross coupling effect, and diverting infrared rays incident on the solar cell.

The HSC proposed in this paper can be used for power generation in space as well as on the ground and is applicable to a wavelength multiplexer/demultiplexer used in optical communication and a diffraction window for indoor lighting.

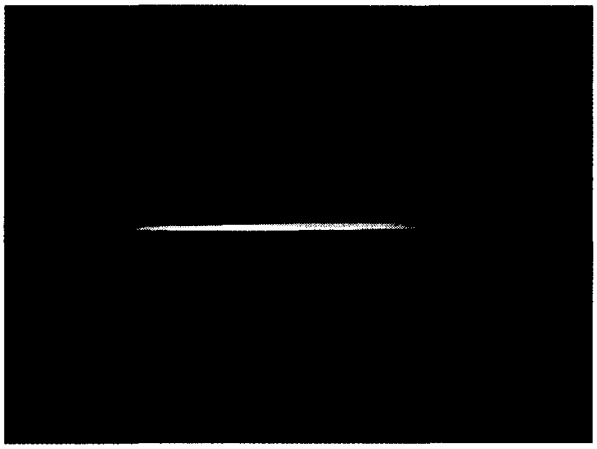

FIG. 11. The reconstructed image of the HSC on the image plane.

REFERENCES

[1] J. L. Stone, Phys. Today 22 (1993).

[2] D. V. Pulfrey, *Photovoltaic Power Generation* (Van Nostrand Reinhold Comp., New York, 1978).

[3] J. E. Ludman, N. O. Reinhand, and I. V. Semenova, SPIE **2108**, 514 (1993).

[4] J. E Ludman, J. Riccobono, I. V. Semenova, N. O. Reinhard, W. Tai, X. Li, G. Syphers, E. Rallis, G. Sliker, and J. Martin, J. Solar Energy **60**, 1 (1997).

[5] N. O. Reinhand, I. V. Semenova, J. Ludman, and J. Riccobono, J. Opt. Technol. **64**, 336 (1997).

[6] J. R. Riccobono, J. E. Ludman, U. S. Pat. No. 5517339 (1996).

[7] H. Kogelnik, Bell Syst. Tech. J. **48**, 2909 (1969).

[8] W. T. Welford, *Aberrations of Optical Systems* (Adam Hilger Ltd., Bristo, 1986) pp. 75-78.

[9] H. I. Bjelkhagen, *Silver-Halide Recording Materials* (Springer-Verlag, New York, 1995), Chapters 3–5.